RSC Advances

PAPER

View Article Online
View Journal | View Issue

Cite this: *RSC Adv.*, 2026, **16**, 25131

pH-responsive sodium alginate/CMCS/CMCNa composite hydrogel beads for sustained delivery of 5-fluorouracil-β-cyclodextrin inclusion complexes

Yaling Wu,[a] Peipei Xu,[ac] Jing Lin,[ac] WanJing Li,[a] Qing Lin,[a] Hanhao Lu,[b] Jingbo Chen,*[b] Zhenhua Liu*[b] and Yudong Lu*[c]

Received 8th January 2026
Accepted 16th April 2026

DOI: 10.1039/d6ra00194g

rsc.li/rsc-advances

Colorectal cancer chemotherapy often faces challenges such as rapid drug clearance, non-specific biodistribution, and burst release, leading to systemic toxicity and reduced therapeutic efficacy. To overcome these limitations, this study developed a colon-targeted sustained-release hydrogel bead system based on β-cyclodextrin (β-CD) and biocompatible polymers (CMCS/CMCNa/SA). The results demonstrated that the incorporation of β-CD significantly enhanced the drug loading capacity through host–guest interactions. Under the optimal mass ratio of drug complex to wall material (15 : 35), the encapsulation efficiency reached as high as 81.23%. Drug release kinetics showed high correlation coefficients (R^2 > 0.9) in zero-order, first-order, Higuchi, and Korsmeyer–Peppas models, indicating a diffusion-controlled release mechanism. The β-CD-modified hydrogel matrix effectively sustained the release of 5-fluorouracil (5-Fu) within the therapeutic window while minimizing the initial burst release. In conclusion, this intelligent delivery system takes advantage of the host–guest inclusion of β-CD and the pH-responsive properties of the polymers, showing promise for localized treatment of colorectal cancer.

1 Introduction

Colorectal cancer is an adenocarcinoma that may progress to a malignant tumor if not treated properly.[1,2] The FOLFOX regimen (comprising 5-fluorouracil, leucovorin, and oxaliplatin) is a preferred chemotherapy option for colorectal cancer.[3] 5-Fluorouracil (5-Fu) plays a significant role in clinical therapy and serves as the gold-standard drug for the treatment of tumors in the gastrointestinal tract (including colorectal, pancreatic, and gastric cancers) and the genitourinary system (such as ovarian and prostate cancers).[4,5] However, its clinical application is restricted by several limitations,[6,7] primarily characterized by a brief half-life, notable toxicity, and low bioavailability. In recent years, gel spheres derived from natural polysaccharides have garnered substantial interest due to their outstanding biocompatibility, biodegradability, and ability to control drug release.[8,9] The use of biodegradable polymer carriers has the potential to markedly enhance the clinical efficacy of 5-fluorouracil by regulating its release rate. This approach can lead to improved oral bioavailability, prolonged half-life, reduced toxicity, minimized gastrointestinal irritation, better patient adherence, and decreased drug wastage.

To prevent the degradation of the active substance in the stomach before it reaches the intestine, it is essential to design carrier systems capable of responding to the pH variations between the gastric and intestinal environments.[10] At present, carrier systems utilizing pH-sensitive materials have gained widespread acceptance. These systems maintain stability in the acidic milieu of the stomach and enable precise drug release under the neutral or weakly alkaline conditions of the intestine.[11] Sodium alginate (SA), a natural anionic polysaccharide, can be crosslinked with divalent cations such as Ca^{2+} to form delivery systems suitable for bioactive substances.[12,13] The SA hydrogel demonstrates remarkable pH–sensitive properties attributed to its abundant carboxyl groups, which undergo ionization in acidic conditions and deprotonation in alkaline environments.[14] However, the system is hindered by three significant limitations: low drug encapsulation efficiency, susceptibility to drug leaching, and burst release of the drug due to the dissolution of SA in the alkaline environment of the intestine.[15] To address these challenges, two improvement strategies have been proposed. First, sodium alginate (SA) was combined with other polymers to enhance its performance.[16] Second, 5-Fu was encapsulated within β-cyclodextrin (β-CD) to

[a]*School of Materials and Chemical Engineering, Fuzhou Institute of Oceanography, Minjiang University, Fu-zhou, Fujian 350108, China. E-mail: 2934@mju.edu.cn*

[b]*Department of Oncology, Shengli Clinical Medical College of Fujian Medical University, Fujian Provincial Hospital, Fuzhou University Affiliated Provincial Hospital, Fuzhou, 350001, China. E-mail: cjbfjsl@fjmu.edu.cn; liuzhenhua6909@163.com*

[c]*College of Chemistry and Materials Science, Fujian Provincial Key Laboratory of Advanced Oriented Chemical Engineer, Fujian Key Laboratory of Polymer Materials, Fujian Normal University, Fuzhou, Fujian 350117, China. E-mail: luyd@fjnu.edu.cn; Tel: (+86) 156-5916-8406*

construct a dual-sustained-release drug delivery system. Carboxymethyl chitosan (CMCS) exhibits remarkable pH sensitivity owing to the ionization of its acidic groups. CMCS hydrogels swell under higher pH conditions and demonstrate pronounced pH responsiveness, enabling targeted drug release in the alkaline environment of the intestine.[14] Carboxymethyl cellulose sodium (CMCNa) has been extensively employed in biomedical applications owing to its remarkable hydrophilicity, biocompatibility, biodegradability, and pH sensitivity.[17] These properties render CMCNa an ideal material for drug delivery systems, as it can facilitate the controlled release of therapeutic agents and enhance their bioavailability.[18,19] β-Cyclodextrin (β-CD) is composed of seven D-glucopyranose units linked by α-1,4-glycosidic bonds, forming a cyclic structure.[20] Its unique hydrophobic cavity enables the formation of inclusion complexes with 5-Fu.[21,22] Additionally, β-CD can enhance the stability and solubility of drugs, while its molecular surface contains numerous hydroxyl groups that can chelate with heavy metal ions to form complexes.[23]

Building upon these foundations, this study developed an innovative 5-fluorouracil (5-Fu) delivery system through the rational design of β-cyclodextrin-encapsulated hydrogel spheres (β-CD@5-Fu/Gel). The system synergistically integrates three functional polymers: carboxymethyl chitosan (CMCS) for pH-responsive release and antimicrobial activity, carboxymethyl cellulose sodium (CMC-Na) for structural reinforcement, and sodium alginate (SA) for calcium ion-triggered gelation, combined with β-CD inclusion complexes for enhanced drug loading capacity. The carrier materials selected in this study (sodium alginate, carboxymethyl chitosan, sodium carboxymethyl cellulose, and β-cyclodextrin) have been widely reported to possess good biocompatibility. In addition, the antitumor activity of 5-Fu against colorectal cancer cell lines (such as HT-29 and Caco-2) has been well documented in the literature.[24–26] On this basis, this study systematically evaluated the sustained-release mechanism and pharmaceutical characteristics of this multi-component system. The results demonstrated that the encapsulation efficiency of 5-Fu in the β-CD@5-Fu complex was 38.32%, with a drug loading rate of 29.82%. Following further optimization of the preparation process, when the mass ratio of the drug complex to the wall materials (CMCS/CMCNa/SA) was 15 : 35, the resulting hydrogel beads exhibited optimal performance, with the encapsulation efficiency significantly enhanced to 81.23%. Drug release kinetic studies revealed that the hydrogel beads achieved fitting coefficients (R^2) greater than 0.9 in zero-order, first-order, Higuchi kinetic and Korsmeyer–Peppas models, indicating that β-CD could sustainably release the encapsulated drug within a defined range, thereby maintaining a more stable drug concentration and effectively preventing burst release. This characteristic provides critical theoretical and technical support for the colon-targeted delivery and sustained release of 5-Fu. The anticipated outcomes of this study are expected to contribute theoretical and technical insights into the development of a novel 5-Fu delivery system and offer new perspectives for the delivery of other hydrophobic drugs (Scheme 1).

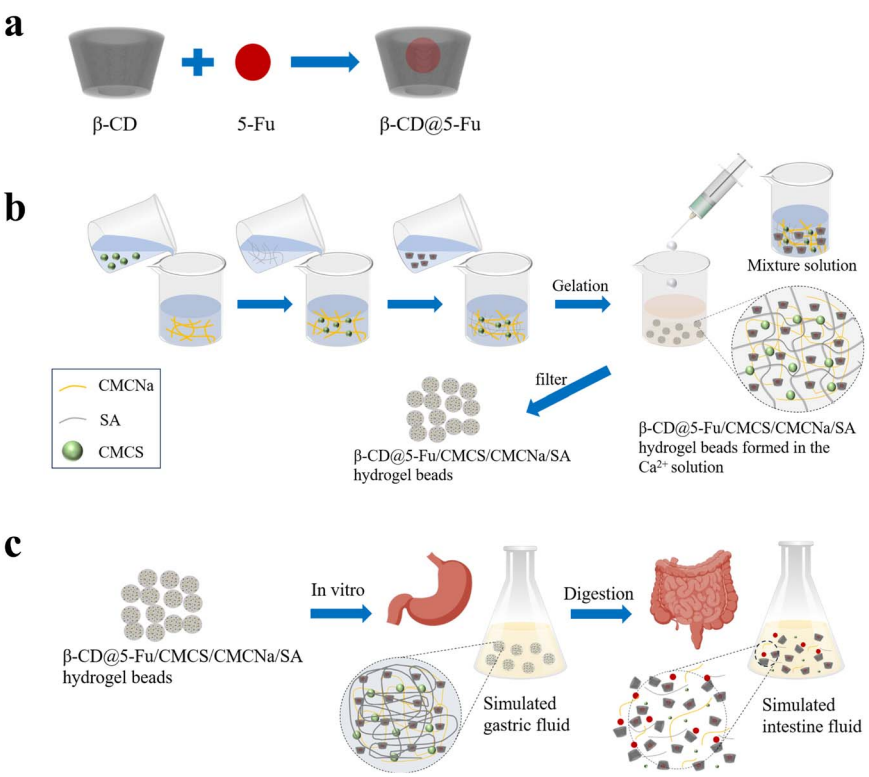

Scheme 1 (a) Synthesis of β-CD@5-Fu; (b) preparation process of β-CD@5-Fu/CMCS/CMCNa/SA hydrogel beads; (c) *in vitro* release mechanism of β-CD@5-Fu/CMCS/CMCNa/SA hydrogel beads.

2 Materials and methods

2.1. Materials

β-Cyclodextrin (β-CD) and sodium alginate (SA) were purchased from Shanghai Aladdin Biochemical Technology, Carboxymethyl chitosan (CMCS), carboxymethyl cellulose sodium (CMCNa), calcium chloride ($CaCl_2$), and sodium chloride (NaCl) were obtained from Sinopharm Chemical Reagent, 5-fluorouracil (5-Fu) was acquired from Shanghai Macklin Biochemical Technology.

2.2. β-CD@5-Fu inclusion complex

The experimental procedure was adapted from the methodology reported by Daria L. Melnikova *et al.*[27] Initially, 3 grams of cyclodextrin were precisely weighed and dissolved in 100 mL of purified water. The mixture was continuously stirred at 80 °C until a homogeneous, clear solution was achieved, yielding a 3% β-CD solution. To prepare the β-CD@5-Fu inclusion complex, 50 mL of the 3% β-CD solution (equivalent to 1.5 g of β-CD) was mixed with 50 mL of a 10^{-1} mol L^{-1} 5-Fu solution (containing 0.6504 g of 5-Fu) at a 1 : 1 volume ratio. The combined mixture was then subjected to ultrasonication at 80 W for 1 hour using an ultrasonic device while being sealed with plastic wrap to prevent evaporation. Subsequently, the mixture was refrigerated at 4 °C for 12 hours to facilitate the formation of the inclusion complex. After refrigeration, the mixture was filtered to isolate the supernatant, which was preliminarily frozen at −80 °C and subsequently lyophilized for 24 hours to obtain the final β-CD@5-Fu powder.

2.3. β-CD@5-Fu/CMCS/CMCNa/SA hydrogel beads

Hydrogel beads of β-CD@5-Fu/CMCS/CMCNa/SA were synthesized following a meticulous protocol based on the ratios outlined in Table S1. Precise quantities of 3% β-CD@5-Fu solution, 3% CMCNa solution, 3% CMCS solution, and 3% SA solution were combined to form the mixture. This mixture underwent sonication at 80 W power for 1 hour using a numerically controlled ultrasonic cleaner to ensure homogeneous dispersion. Subsequently, the mixture was subjected to hydration at 4 °C in a refrigerated environment for 2 hours, allowing complete molecular interaction and stabilization.

Following this, the resultant β-CD@5-Fu/CMCS/CMCNa/SA mixture was carefully dispensed using a 5 mL syringe into a 2% calcium chloride ($CaCl_2$) solution for crosslinking. The crosslinking process was maintained for 12 hours at ambient temperature, facilitating the formation of spherical hydrogel beads through ionic interaction between the alginate and calcium ions. The synthesized β-CD@5-Fu/CMCS/CMCNa/SA hydrogel beads were then preserved in 0.9% sodium chloride (physiological saline) solution and stored at 4 °C to maintain structural integrity and stability for further characterization and application studies.

2.4. Encapsulation efficiency and loading capacity

2.4.1. β-CD@5-Fu inclusion complex. Approximately 0.010–0.015 g of the inclusion complex sample was dispersed in 3 mL of PBS buffer solution (pH 7.4). Under ultrasonication, 5-Fu was efficiently extracted from the inclusion complex into the PBS buffer solution for 10 minutes. The mixture was then subjected to centrifugation at 4000 rpm for 10 minutes to separate the supernatant, which contained the released 5-Fu. The concentration of 5-Fu in the supernatant was quantified using UV spectrophotometry at a wavelength of 264 nm, with reference to a standard calibration curve of 5-Fu. Based on the measurements, the encapsulation efficiency (EE%) and loading capacity (LC%) were calculated using the following formulas:

$$\mathrm{EE}(\%) = \frac{\text{Amount of 5-Fu actually encapsulated}}{\text{Total amount of5-Fu added}} \times 100 \quad (1)$$

$$\mathrm{LC}(\%) = \frac{\text{Amount of 5-Fu actually encapsulated}}{\text{Total mass of carrier}} \times 100 \quad (2)$$

2.4.2. β-CD@5-Fu/CMCS/CMCNa/SA hydrogel beads. An appropriate amount of β-CD@5-Fu/CMCS/CMCNa/SA HMs sample was dispersed in PBS solution (pH 7.4), then sonicated for 5 minutes, followed by continuous stirring for 2 hours to extract 5-Fu. The reloaded β-CD@5-Fu/CMCS/CMCNa/SA hydrogel beads require crushing prior to extraction. The suspension was centrifuged at 4500 rpm for 10 minutes, and the absorbance of the supernatant was measured at 264 nm. The total amount of 5-Fu was calculated from the standard curve. The encapsulation efficiency (EE) and loading capacity (LC) were calculated as follows, and the encapsulation efficiency and drug loading were calculated using the standard curve of 5-Fu. They were calculated as follows (eqn (3) and (4)):

$$\mathrm{EE}(\%) = \frac{\text{Weight of 5-Fu in the HMs}}{\text{Theoretical weight of 5-Fu}} \times 100 \quad (3)$$

$$\mathrm{LC}(\%) = \frac{\text{Weight of 5-Fu in the HMs}}{\text{Weight of 5-Fu/HMs}} \times 100 \quad (4)$$

2.5. Characterization of β-CD@5-Fu inclusion complex

2.5.1. Ultraviolet (UV). The inclusion complex was analyzed using a UV-Vis spectrophotometer (UV1902, Cold Light Technology, Shanghai, China) with a wavelength range of 200–600 nm.

2.5.2. Fourier transform infrared spectroscopy (FT-IR) analysis was performed. The hydrogel beads were characterized using Fourier Transform Infrared Spectroscopy (FT-IR) (ATR-FTIR, Nicolet 5700, Thermo Fisher Scientific, USA). The hydrogel beads were mixed with KBr at a ratio of 1 : 100 (g g^{-1}) and pressed into pellets. The spectrum was scanned and recorded in the range of 4000–400 cm^{-1}.

2.5.3. X-Ray diffraction (XRD). X-Ray diffraction (XRD) (XRD, Rigaku SmartLab SE, Japan) analysis was performed using a Rigaku SmartLab SE diffractometer with Cu Kα radiation ($\lambda = 0.15406$ nm) at 40 kV. The 2θ range was set from 10° to 80°, and the scanning rate was 2.0° min^{-1}.

2.6. Characterization of β-CD@5-Fu/CMCS/CMCNa/SA hydrogel beads

2.6.1. Fourier transform infrared spectroscopy (FT-IR) testing. The chemical structure of the drug-loaded hydrogel

beads was detected using a Fourier Transform Infrared Spectrometer. In sample preparation, a small amount of the dried sample powder was mixed uniformly with KBr powder and then pressed into a pellet at room temperature. The spectrum was scanned and recorded in the range of 4000–400 cm^{-1}.

2.6.2. Simultaneous thermal analysis (TG-DSC). The inclusion complex and hydrogel samples were heated from room temperature to 600 °C at a heating rate of 10 °C min^{-1} under a nitrogen atmosphere. The thermogravimetric (TG) and differential scanning calorimetry (DSC) curves were recorded simultaneously to analyze the mass changes and thermal effects of the samples during the heating process.

2.6.3. Scanning electron microscopy (SEM). The surface morphology of the freeze-dried hydrogel beads was observed using a scanning electron microscope (SEM, ZEISS Sigma 360). The freeze-dried hydrogel beads were fixed on a conductive carbon tape and sputter-coated with a thin layer of gold before observation.

2.6.4. Swelling ratio (SR). The dried (dry beads) and undried (wet beads) β-CD@5-Fu/CMCS/CMCNa/SA hydrogel beads were weighed separately, and their masses were recorded as W_d. They were then immersed in 10 mL of different swelling media for 24 h to allow swelling. After swelling, the hydrogel beads were removed, gently blotted with filter paper to remove excess surface water, and immediately weighed, recorded as W_t. The swelling ratio (SR) was calculated using the following equation:

$$\mathrm{SR}(\%) = \frac{W_t - W_d}{W_d} \times 100 \quad (5)$$

W_d: initial weight of the hydrogel beads (g); W_t: wet weight of the hydrogel beads at time t (g).

2.7. *In vitro* drug release and kinetic analysis

The *in vitro* drug release study was conducted following a modified protocol from literature.[28] Experimental conditions were maintained at 37 °C using simulated physiological fluids: gastric fluid (pH 1.5) and intestinal fluid (pH 6.8). Precisely weighed hydrogel samples (0.5 g) were immersed in 10 mL of release medium. At predetermined time points, 2 mL aliquots of the medium were systematically withdrawn and immediately replaced with equal volumes of fresh medium to preserve sink conditions. UV-Vis spectrophotometric measurements were performed at $\lambda = 264$ nm to determine absorbance values, from which the cumulative 5-fluorouracil release (CFR) was calculated according to eqn (6). To evaluate the stability of the system before reaching the colon, we simulated gastric conditions (pH 1.2), upper gastrointestinal tract conditions (pH 6.8, with and without phosphate), and colonic conditions (pH 7.4, with and without phosphate), and investigated the release behavior of the hydrogel beads in different media. The release experiment was conducted using the replacement method, in which 2 mL of sample was withdrawn at each time point, followed immediately by the addition of an equal volume of fresh medium at the same temperature to maintain a constant total volume of 10 mL. All experimental procedures were executed in triplicate to ensure data reproducibility.

$$\mathrm{CFR}(\%) = \frac{\sum_{i=0}^{n}(C_i V_i)}{W} \times 100 \quad (6)$$

where C_i is the concentration of the target substance in the release medium measured at the ith time point (unit: mg mL^{-1}), V_i is the volume sampled at the ith time point (unit: mL), and W (mg) is the total loading mass of 5-Fu in the hydrogel.

To investigate the release mechanism of 5-Fu from the prepared hydrogel, the drug release data were analyzed using zero-order kinetic model (eqn (7)), first-order kinetic model (eqn (8)), Higuchi model (eqn (9)) and Korsmeyer–Peppas model (eqn (10)). Kinetic models can clearly provide the suggested release mechanism of the drug delivery system.

$$Q_t = Q_0 + K_0 t \quad (7)$$

$$\log Q_t = \log Q_0 + K_1 t \quad (8)$$

$$Q_t = K_H t^{1/2} \quad (9)$$

$$\frac{M_t}{M_\infty} = K t^n \quad (10)$$

Q_t is the cumulative drug release at time t, Q_0 is the initial drug quantity, and t is the time; M_t is the drug release at time t, K is the release constant, $\frac{M_t}{M_\infty}$ is the fraction of drug released at time t; n is release exponent (dimensionless), indicating the drug release mechanism.

2.8. Statistical analysis

All experiments were replicated at least three times, and the data were presented as mean ± standard deviation. Origin 2021 software was employed to analyze and plot the data, and the results were analyzed by variance.

3 Results and discussion

3.1. Characterization of β-CD@5-Fu inclusion complex

The formation of an inclusion complex between the cavity structure of β-cyclodextrin (β-CD) and 5-fluorouracil (5-Fu) is the core mechanism for achieving drug loading and initial stability. The inclusion interaction is maintained through hydrophobic interactions and hydrogen bonding, resulting in the formation of the β-CD@5-Fu inclusion complex. The absorption peak of 5-Fu at 264 nm (ref. 29) is distinct. β-CD exhibits low absorbance at 300 nm. The redshift of the UV absorption peak of the β-CD@5-Fu complex (the compound of β-CD and 5-Fu) from 264 nm to around 266 nm suggests an interaction between β-CD and 5-Fu, indicating successful encapsulation of 5-Fu into the cavity of β-CD (Fig. 1(a)).

FTIR spectroscopy is an exploratory analytical tool used to confirm the formation of inclusion complexes. In β-CD complexes, non-covalent interactions such as hydrophobic interactions, van der Waals forces, and hydrogen bonds

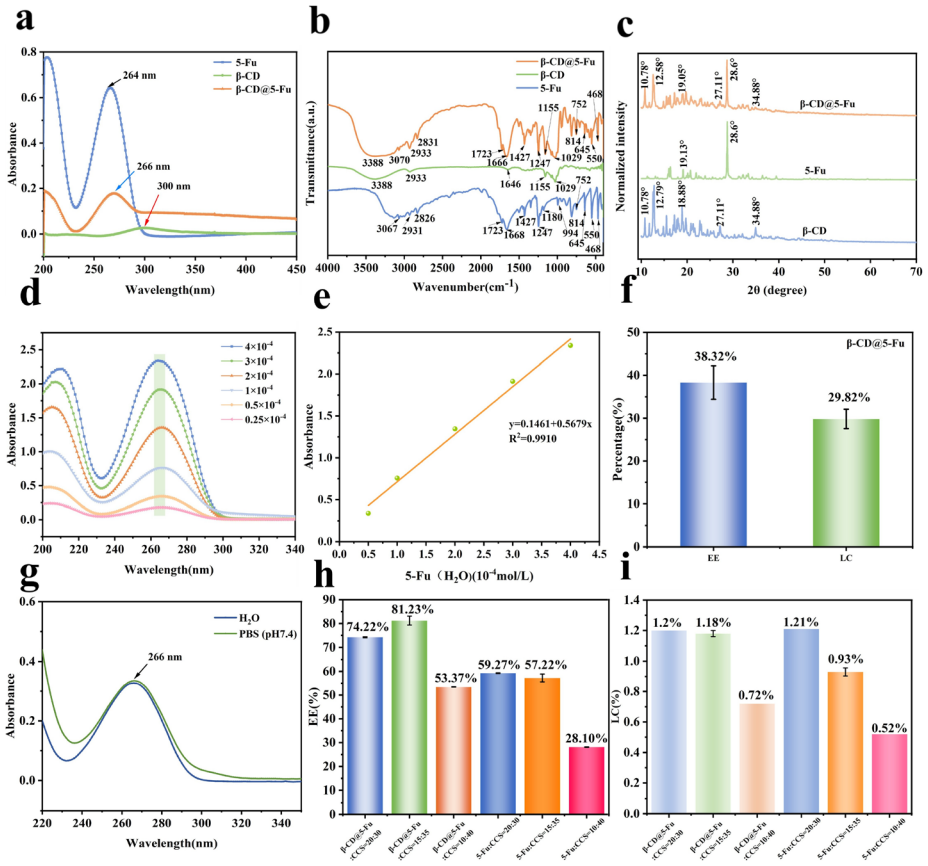

Fig. 1 Characterization of β-CD@5-Fu inclusion complex and drug-loaded hydrogels: (a) UV-Vis spectra of 5-Fu, β-CD, and β-CD@5-Fu; (b) FTIR spectra of 5-Fu, β-CD, and β-CD@5-Fu; (c) XRD patterns of 5-Fu, β-CD, and β-CD@5-Fu; (d) UV-Vis calibration curves of 5-Fu at different concentrations; (e) linear regression of 5-Fu concentration *versus* absorbance; (f) encapsulation efficiency (EE) and drug loading (DL) capacity of β-CD@5-Fu; (g) absorbance comparison of β-CD@5-Fu in water *versus* PBS; (h and i) EE and DL of hydrogel beads with different drug-carrier ratios (w/w).

between β-CD and guest molecules lead to a decrease in the energy of the encapsulated portion of the guest molecules, reducing the intensity of peaks at corresponding frequencies. The FT-IR spectra of 5-Fu, β-CD, and β-CD@5-Fu are shown in Fig. 1(b). The characteristic peaks of β-CD, arising from the glucose macromolecule, are located at 3388 cm^{-1} (O–H stretching), 2933 cm^{-1} (C–H stretching), 1646 cm^{-1} (C=O stretching), and 1155 cm^{-1} (C–O stretching), which are attributed to the glycosidic bonds and hydroxyl groups present in the β-CD molecule.[30] In the structure of 5-Fu, the peaks at 1723 cm^{-1} and 1668 cm^{-1} are attributed to two different carbonyl groups. The broad peak in the range of 2826–3388 cm^{-1} is associated with the NH stretching vibration in 5-Fu. In the FT-IR spectrum of 5-Fu, the peaks at 1427 cm^{-1} and 1247 cm^{-1} correspond to the C–N and C–O stretching modes, respectively. The peak in the range of 1155–1180 cm^{-1} is related to the C–F stretching, while the peak at 752 cm^{-1} is attributed to the vibration of the CF=CH group. The peak at 814 cm^{-1} corresponds to the C–F rocking mode, and the peak at 994 cm^{-1} is assigned to the C=C stretching mode.[31] The FTIR spectrum of the β-CD and 5-Fu complex shows significant changes compared to that of 5-Fu. The C–F stretching band of 5-Fu at 1180 cm^{-1} completely disappears. This is because the drug is encapsulated within the cavity of β-cyclodextrin, forming an inclusion complex. The carbonyl stretching band of 5-Fu (at 1668 cm^{-1}) experiences a moderate blue shift to 1666 cm^{-1} (β-CD@5-Fu), which further confirms the successful formation of the inclusion complex.[27]

5-Fu exhibits sharp diffraction peaks at 19.13° and 28.6°, revealing its crystalline structure (Fig. 1 (c)).[32] The diffraction peaks of β-CD are observed at 2θ = 10.78°, 12.79°, 18.88°, 27.11°, and 34.88°, indicating its crystalline nature.[33,34] The β-CD@5-Fu complex shows sharp diffraction peaks at 10.78°, 12.58°, 19.05°, 27.11°, 28.6°, and 34.88°. In the XRD pattern of β-CD@5-Fu, certain peaks (such as 10.78°, 27.11°, 28.6°, and 34.88°) overlap with the diffraction peaks of β-CD and 5-Fu, suggesting that parts of their original crystalline structures are retained after complexation. This may indicate that the combination of 5-Fu and β-CD forms a stable complex without completely altering their crystalline structures.

As illustrated in Fig. 1(d and e), a good linear relationship of 5-Fu is observed within the concentration range of 0.5 × 10^{-4} to 4.0 × 10^{-4} mol L^{-1}, with the linear equation $y = 0.1461 + 0.5679x$ and a high coefficient of determination ($R^2 = 0.9910$).

Furthermore, as shown in Fig. 1(g), the β-CD@5-Fu inclusion complex exhibits excellent solubility in both aqueous solution and PBS buffer (pH 7.4). Quantitative analysis reveals that the encapsulation efficiency of 5-Fu in the β-CD@5-Fu inclusion complex is 38.32%, with a drug loading capacity of 29.82% (Fig. 1(f)). It should be noted that this relatively low encapsulation efficiency is primarily attributed to the preparation process, in which an excess of 5-Fu (molar ratio of 5-Fu : β-CD ≈ 3.78 : 1) was used during the ultrasound-assisted preparation of the inclusion complex, and the unencapsulated free drug was removed during the subsequent filtration step. Nevertheless, this inclusion complex still provides a sufficient drug loading foundation for the subsequent preparation of hydrogel beads. Through comparative evaluation of six different drug-loaded hydrogel bead formulations (as shown in Fig. 1(h and i)), the sample with a β-CD@5-Fu to CCS (CMCS/CMC-Na/SA) mass ratio of 15 : 35 exhibited the highest encapsulation efficiency, reaching 81.23%. This result indicates that the hydrogel beads achieve optimal drug encapsulation capability at this specific mass ratio. Meanwhile, the corresponding drug loading capacity is 1.18%, further confirming that the optimized mass ratio significantly enhances the effective drug loading capacity, which is sufficient to support the subsequent release behavior characterization and mechanism analysis.

3.2. Characterization of β-CD@5-Fu/CMCS/CMCNa/SA hydrogel beads

To evaluate the formation of the β-CD@5-Fu inclusion complex and its effect on the thermal stability of the hydrogels, thermogravimetric analysis (TGA) was performed on 5-Fu, β-CD, physical mixture, β-CD@5-Fu inclusion complex, CMCS/CMCNa/SA hydrogel beads, and β-CD@5-Fu/CMCS/CMCNa/SA composite hydrogel beads.

As shown in Fig. 2(c) and (d), the physical mixture of 5-Fu and β-CD exhibited three distinct decomposition temperatures at 72.37 °C, 287.83 °C, and 327.54 °C, respectively. In contrast,

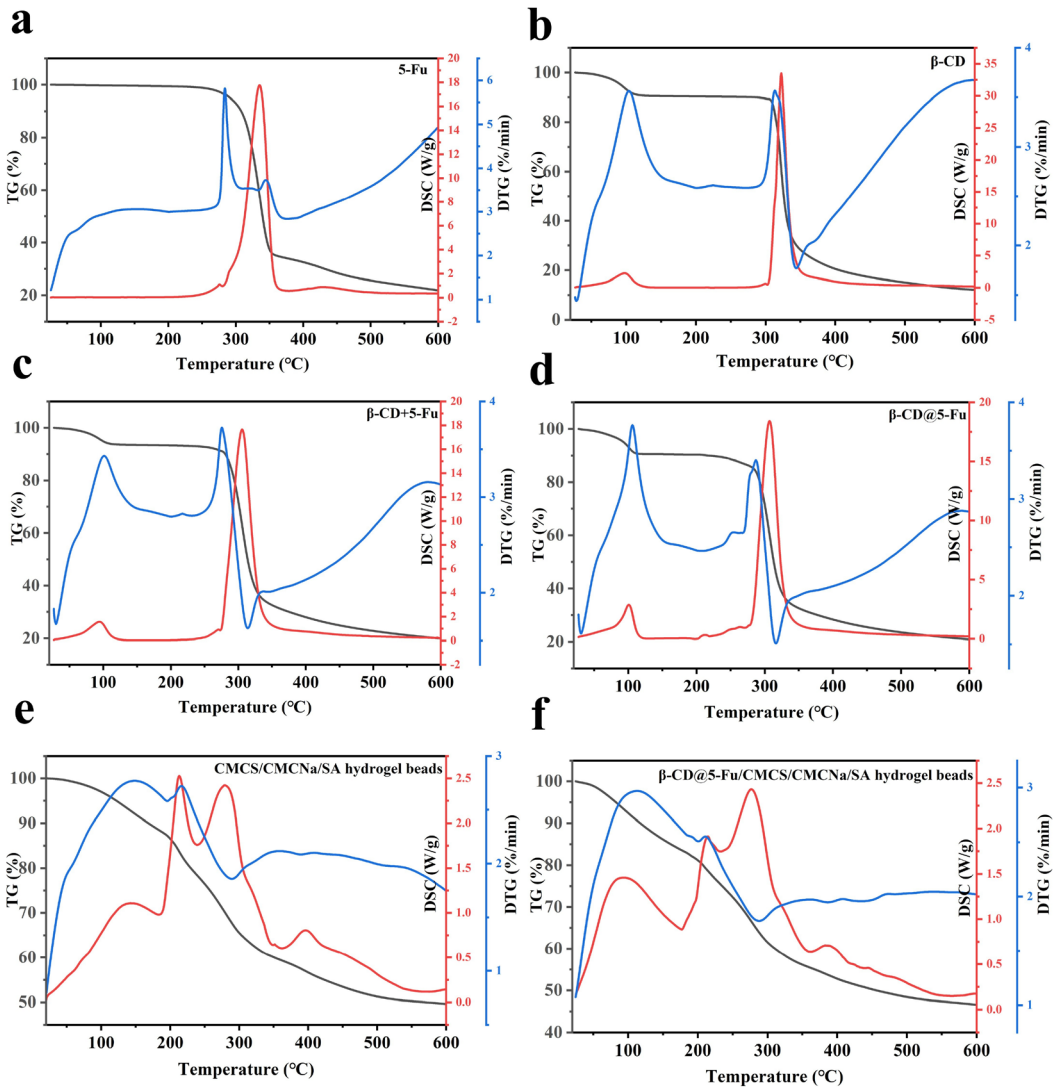

Fig. 2 Simultaneous thermogravimetry-differential scanning calorimetry (TG-DSC) curves of 5-Fu (a), β-CD (b), physical mixture of 5-Fu and β-CD (c), β-CD@5-Fu inclusion complex (d), CMCS/CMCNa/SA hydrogel beads (e), and β-CD@5-Fu/CMCS/CMCNa/SA (f).

the DTG curve of the β-CD@5-Fu inclusion complex displayed significantly different thermal behavior: its onset decomposition temperature decreased to 83.32 °C, the second decomposition step began at 235.77 °C, and the overall decomposition temperature range extended to 83.32–325.46 °C. This thermal behavior was distinctly different from that of the physical mixture, indicating that 5-Fu was successfully encapsulated into the hydrophobic cavity of β-CD, forming a stable inclusion complex. The inclusion interaction, stabilized by hydrogen bonding and hydrophobic interactions, altered the original thermal degradation pathway of 5-Fu.

Further comparison between Fig. 2(e) and (f) revealed that the CMCS/CMCNa/SA hydrogel beads without the inclusion complex exhibited decomposition peaks at 83.83 °C, 201.18 °C, 260.48 °C, and 467.97 °C, with a residual mass of 49.64% upon heating to 600 °C. After loading with the β-CD@5-Fu inclusion complex, the decomposition peaks of the composite hydrogel beads became significantly broader, with decomposition temperatures observed at 55.84 °C, 214.11 °C, 282.29 °C, and 382.82 °C, indicating a markedly expanded thermal decomposition range. However, its final residual mass (46.58%) was slightly lower than that of the hydrogel beads without the inclusion complex (49.64%).

These results indicate that the introduction of the β-CD@5-Fu inclusion complex did not significantly increase the residual mass of the hydrogel at the extreme high temperature (600 °C) but did markedly alter its thermal decomposition behavior. The decrease in onset decomposition temperature (from 83.83–55.84 °C) may be attributed to the premature release of bound water within the β-CD cavity of the inclusion complex.[35] Meanwhile, the increase and broadening of the decomposition peaks reflect the formation of more complex non-covalent interactions (such as hydrogen bonding and hydrophobic interactions) between the inclusion complex and the hydrogel matrix, resulting in a multi-stage thermal decomposition process.[36]

In the hydrogel network composed of sodium alginate (SA), carboxymethyl chitosan (CMCS), and sodium carboxymethyl cellulose (CMCNa), there are abundant $-COO^-$, $-NH_3^+$, –OH, and –COOH groups. The interactions formed among these groups are the main forces maintaining the stability of the three-dimensional gel structure. The FTIR analysis results showed that the characteristic absorption peaks of the samples were consistent in position but varied in intensity. Specifically, the characteristic absorption peaks of CMCS/CMCNa/SA, SA, CMCS, and CMCNa appeared at 3436 cm^{-1} (O–H stretching vibration), 2923 cm^{-1} (C–H stretching vibration), 1603 cm^{-1} (C═O stretching vibration), 1429 cm^{-1} (C═C stretching vibration), and 1036 cm^{-1} (C–O stretching vibration).[37] Additionally, the absorption peaks observed at 707 cm^{-1} and 817 cm^{-1} can be

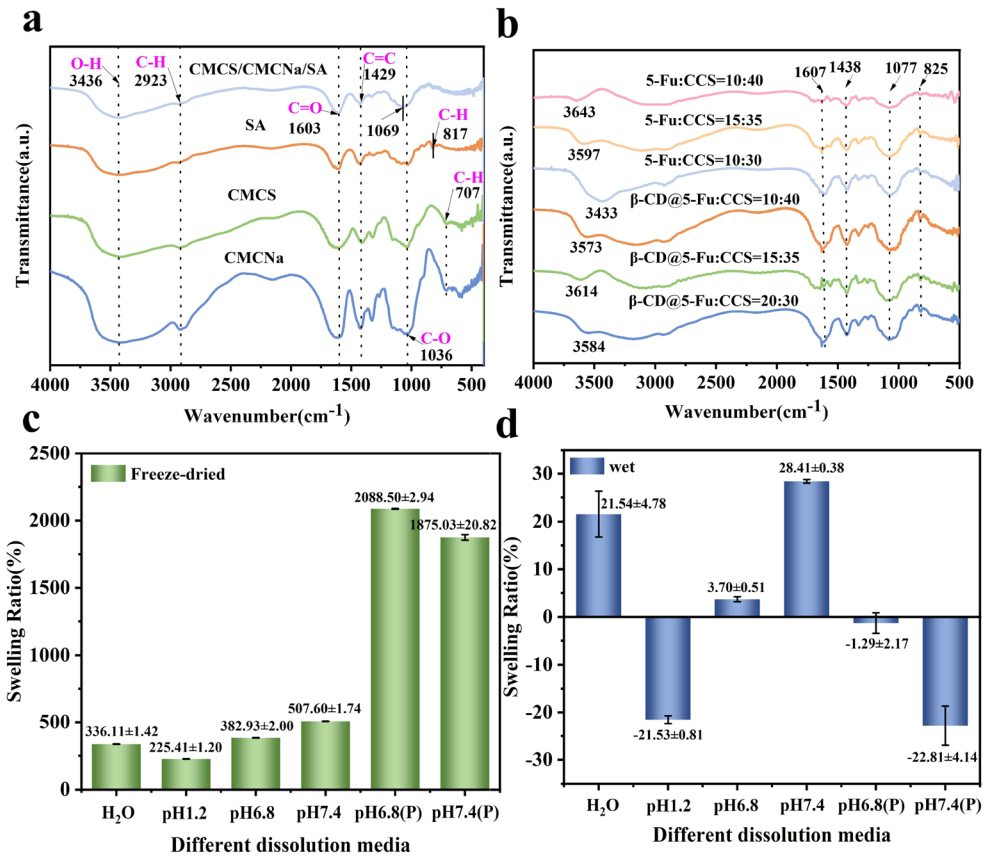

Fig. 3 (a) FTIR spectra of raw materials; (b) FTIR spectra of six hydrogel bead formulations; swelling ratio of β-CD@5-Fu/CMCS/CMCNa/SA hydrogel dried beads (c) and swollen beads (d) in purified water and under different pH conditions (pH 1.2; pH 6.8 with and without phosphate; pH 7.4 with and without phosphate) at 37 °C for 24 h.

attributed to the characteristic C–H bending vibrations.[38] Notably, a redshift of the characteristic absorption peak of the CMCS/CMCNa/SA hydrogel beads from 1036 cm^{-1} to 1069 cm^{-1} was observed, which may be associated with the crosslinking of the –COOH groups with Ca^{2+} (Fig. 3(a)). When the drug 5-Fu and β-CD@5-Fu were incorporated into the wall material, a slight broadening of the O–H stretching vibration band in the range of 3433–3643 cm^{-1} was observed, likely due to enhanced hydrogen bonding interactions caused by the addition of 5-Fu and β-CD@5-Fu, resulting in minor changes in the O–H vibration frequency. The peak at 1607 cm^{-1}, which is close to the previously mentioned C=O stretching vibration peak at 1603 cm^{-1}, can be assigned to the C=O stretching vibration. The slight increase in the wave number of the C=C stretching vibration peak at 1438 cm^{-1} may be due to changes in the molecular structure caused by the introduction of the drug or complex, affecting the vibration frequency of the C=C bond. Significant increases in the wave numbers of the C–O stretching vibration peak at 1077 cm^{-1} and the C–H bending vibration peak at 825 cm^{-1} were also observed, likely due to the incorporation of the drug or complex (Fig. 3(b)).

As shown in Fig. 3, the swelling behavior of β-CD@5-Fu/CMCS/CMCNa/SA hydrogel beads exhibited significant pH dependence. The wet hydrogel beads showed exceptionally high swelling ratios across different media. In non-phosphate systems, the swelling ratio reached a maximum of 507.60% at pH 7.4, while it decreased to 225.41% under acidic conditions at pH 1.2, indicating that the hydrogel possesses superabsorbent capacity under physiological conditions, and its pH-responsive nature is favorable for drug release in the intestinal environment. Notably, in phosphate-buffered saline (PBS), the swelling performance of the wet hydrogel was significantly enhanced, with swelling ratios reaching as high as 2088.50% at pH 6.8 PBS and 1875.03% at pH 7.4 PBS, both substantially higher than that in deionized water (336.11%). This phenomenon can be attributed to the ionic strength effect and osmotic pressure effect of PBS, where ions screen the electrostatic interactions between polymer chains, promoting further expansion of the hydrogel network.

In contrast, the freeze-dried hydrogel beads exhibited significantly reduced swelling capacity. In deionized water, the swelling ratio of the freeze-dried beads was only 21.54%. At pH 6.8 and pH 7.4, the swelling ratios were 3.70% and 28.41%, respectively, much lower than those of the wet hydrogel. More importantly, in phosphate-buffered saline, the freeze-dried beads exhibited negative swelling: the swelling ratio was −1.29% at pH 6.8 PBS and decreased to −22.81% at pH 7.4 PBS, indicating substantial mass loss. This may be attributed to the fragile structure formed during freeze-drying, leading to partial disintegration or leaching of soluble components upon rehydration in PBS.

The dramatic difference in swelling behavior between wet and freeze-dried beads suggests that the initial hydration state of the hydrogel plays a decisive role in its subsequent swelling performance. The wet hydrogel, with its pre-formed hydrated network, relaxed polymer chains, and fully exposed hydrophilic groups, can further absorb substantial amounts of water. In contrast, freeze-drying may induce irreversible aggregation of polymer chains or structural embrittlement, where ice crystal formation disrupts network integrity, thereby severely impairing the re-swelling capability. In summary, the hydrogel system exhibits excellent pH responsiveness and superabsorbent capacity in the wet state, with particularly enhanced swelling performance in PBS environments, demonstrating great potential as an intestinal-targeted drug delivery carrier.

The surface morphology of various hydrogel systems was systematically characterized using scanning electron microscopy (SEM), with comparative micrographs of SA, CMCS/CMCNa/SA, 5-Fu/CMCS/CMCNa/SA, and β-CD@5-Fu/CMCS/CMCNa/SA nanocarriers presented in Fig. 4. The SA hydrogel displays a distinct scaly morphology characterized by a regular arrangement of spherical microporous structures, which are indicative of effective swelling behavior and enhanced drug-loading capacity. Following the incorporation of both CMCS and CMCNa, the resulting CMCS/CMCNa/SA hydrogel exhibits a more intricate three-dimensional reticular network, accompanied by an increased specific surface area that suggests superior drug-loading performance. Notably, the 5-Fu-loaded hydrogel formulations demonstrate significantly smoother surface topography with the absence of observable pores, providing compelling evidence for the successful encapsulation of 5-Fu within the polymeric. The surface morphology of the samples is presented in Fig. S1, revealing distinct structural features of hydrogel beads. As shown in Fig. S1(a, c, e, m and o), the hydrogel beads demonstrate ideal spherical geometries with high size uniformity. In contrast, Fig. S1(g, i and k) exhibits significant variations in bead size and deviations from spherical morphology. These morphological differences can be attributed to the unique amphiphilic properties of β-cyclodextrin, whose hydrophobic cavity and hydrophilic exterior facilitate complex interactions with various hydrogel components, including polymer chains and solvent molecules. These interactions, mediated primarily by van der Waals forces and hydrogen bonding, promote hydrogel aggregation while simultaneously stabilizing the spherical architecture of the beads.

From Fig. S2(a), the influence of component ratio on viscosity can be observed. For the β-CD@5-Fu : CCS system, when the CCS ratio increased (from 20 : 30 to 10 : 40), the viscosity showed a non-monotonic increase: from 20 : 30 to 15 : 35, the viscosity rose from 541.96–576.16 mPa s (+6.3%), possibly due to the enhanced entanglement of CCS molecular chains. From 15 : 35 to 10 : 40, the viscosity further increased from 576.16–658.62 mPa s (+14.3%), but it remained lower than that of the 5-Fu : CCS system at the same ratio (698.9 mPa s), suggesting that β-CD inclusion may reduce intermolecular interactions. For the 5-Fu : CCS system, the viscosity first increased significantly and then slightly decreased with the increase of CCS ratio: from 20 : 30 to 15 : 35, the viscosity surged from 653.68–744.68 mPa s (+13.9%), indicating that the increase in CCS concentration significantly enhanced the network density. From 15 : 35 to 10 : 40, the viscosity decreased to 698.9 mPa s (−6.1%), possibly due to local inhomogeneity caused by excessive crosslinking. The 3% SA (sodium alginate) showed the highest viscosity (2600 mPa s), owing to the high

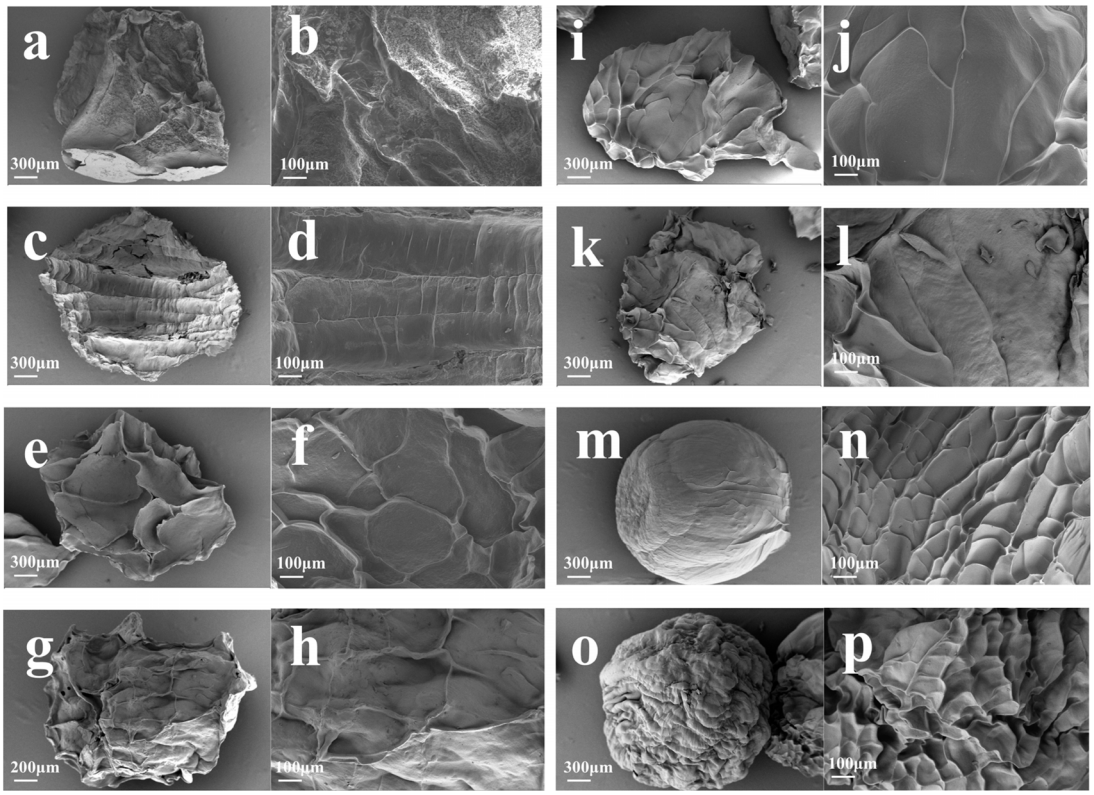

Fig. 4 Scanning electron microscopy (SEM) images of hydrogel beads with different formulations: (a–f) β-CD@5-Fu-loaded hydrogel beads with varying mass ratios of β-CD@5-Fu to CCS: (a and b) 20 : 30, (c and d) 15 : 35, and (e and f) 10 : 40. (g–l) 5-Fu-incorporated hydrogel beads (without β-CD) at corresponding ratios: (g and h) 20 : 30, (i and j) 15 : 35, and (k and l) 10 : 40. (m–p) Control groups: (m and n) pure SA hydrogel beads and (o and p) CMCS/CMC-Na/SA ternary hydrogel beads (without drugs).

entanglement ability of its linear molecular chains. The 3% CMCNa (carboxymethyl cellulose sodium) had the next highest viscosity (1157.5 mPa s), and its anionic property led to the extension of molecular chains. CMCS (carboxymethyl chitosan) had the lowest viscosity (213.25 mPa s), possibly because the lower molecular weight or charge shielding effect weakened the interchain interactions. For the composite matrix (CCS), the viscosity of CCS (SA : CMCNa : CMCS = 1 : 1 : 1) was 1107.5 mPa s, which was between that of CMCNa and CMCS, indicating that SA and CMCNa dominated the viscosity behavior, and the addition of CMCS might interfere with the continuous network structure of SA/CMCNa. The viscosity of the β-CD@5-Fu system was generally lower than that of the directly mixed 5-Fu : CCS system, suggesting that β-CD might reduce the direct contact of polymer chains through steric hindrance.

To further examine the rheological property changes of hydrogel bead precursor solutions and raw hydrates, the variations of storage modulus (G') and loss modulus (G'') with frequency are shown in Fig. S2(b)–(d). The frequency sweep results indicate that both the hydrogel bead precursor solutions and raw hydrates exhibit viscoelastic fluid behavior ($G'' > G'$), without forming a strong gel network. The modulus of raw hydrates is close to that of the precursor solutions, implying that they have already possessed a micro-structure similar to weak gels, possibly due to pre-existing hydration.

3.3. *In vitro* release and kinetic analysis

During the release process, 5-Fu molecules must diffuse out of the β-CD structural framework. The inclusion complex formed between β-CD and 5-Fu restricts the molecular mobility of the drug. This molecular confinement leads to a significant reduction in the release rate, as evidenced by the release profiles in Fig. 5(a) and (b). To further elucidate the release kinetics, the experimental data were analyzed using various kinetic models, and the corresponding fitting parameters are presented in Table 1.

To evaluate the applicability of various kinetic models in describing the drug release behavior, the coefficient of determination (R^2) was employed as a quantitative indicator, where an R^2 value approaching unity signifies an optimal fit to the experimental data. Among the tested models, the zero-order kinetic model demonstrated superior fitting performance, particularly in cases ①, ②, and ④with R^2 values approaching 1. Notably, in cases ①, ②, and ④, the R^2 values exceeded 0.9 for zero-order, first-order, Higuchi kinetic and Korsmeyer–Peppas models, suggesting that the release mechanism is complex and potentially influenced by multiple factors. These findings indicate that β-CD enables sustained drug release within a defined range, which is crucial for maintaining stable drug concentrations and effectively mitigating burst release phenomena.

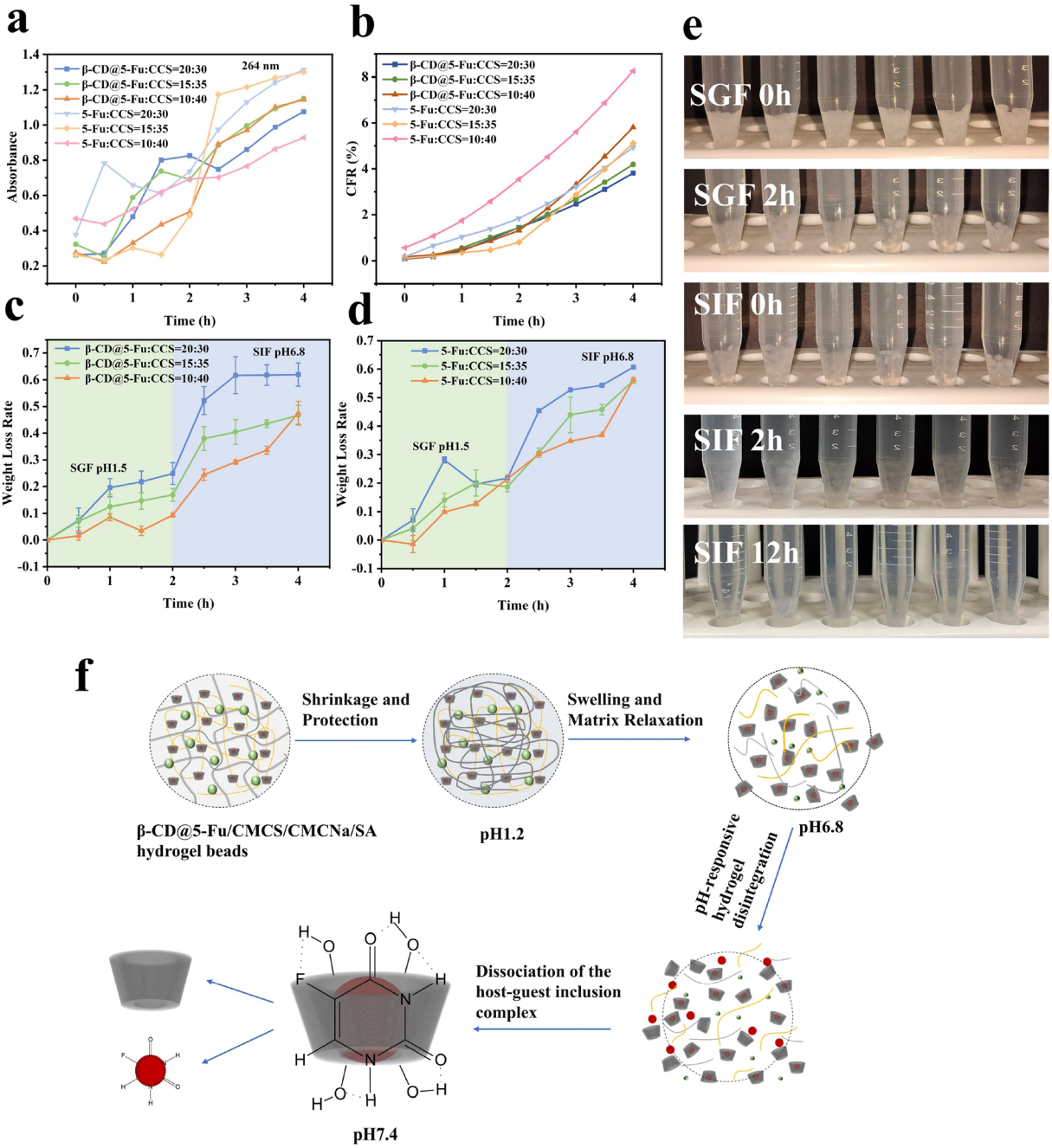

Fig. 5 Drug release performance: (a) release kinetics; (b) shows the comparison results of the cumulative release rate (CFR) of six different hydrogel beads; (c and d) *in vitro* release of β-CD@5-Fu and 5-Fu loaded hydrogels at different ratios (the error bars represent the standard deviation of three replicate experiments); (e) structural stability in SGF (0–2 h) and SIF (0–12 h); (f) schematic diagram of the drug release mechanism from hydrogel beads.

In the Korsmeyer–Peppas model, the release exponent n can be used to determine the drug release mechanism: when $n \leq 0.45$, the drug release mechanism is mainly Fickian diffusion (*i.e.*, simple diffusion). When $0.45 < n < 0.89$, it is non – Fickian diffusion, which is a mixed mechanism of diffusion and polymer matrix erosion. When $n \geq 0.89$, the mechanism is mainly polymer matrix erosion. From the Table 2, the n values of ④ and ⑥ (1.2654 and 1.1569) are relatively small, but both are greater than 0.89. This indicates that in the corresponding samples, the drug release is mainly based on the polymer matrix erosion mechanism. The n values of ①, ②, ③, and ⑤ are even larger, also suggesting that the drug release mainly relies on the polymer matrix erosion mechanism. Moreover, the differences in n values among different ratios of the β-CD@5-Fu and CCS mixed systems, as well as the 5-Fu and CCS mixed systems, reflect the influence of component ratios on the drug release mechanism and rate.

Fig. 5(e) shows optical microscopy images of the *in vitro* digestive behavior of hydrogel beads in simulated gastric fluid (SGF, 0–2 h) and simulated intestinal fluid (SIF, 0–12 h). The

Table 1 Kinetic models used to fit the release data

		Coefficient of determination (R^2)					
Kinetic models	Equations	①	②	③	④	⑤	⑥
Zero-order kinetic model	(6)	0.9975	0.9935	0.9614	0.9956	0.9250	0.9757
First-order kinetic mode	(7)	0.9339	0.9190	0.9442	0.9389	0.9601	0.9941
Higuchi	(8)	0.9308	0.9637	0.8546	0.9512	0.7370	0.8410
Korsmeyer–Peppas	(9)	0.9986	0.9982	0.9970	0.9874	0.9930	0.9901

Table 2 Comparison of fitting parameters and release exponent (n) in the Korsmeyer–Peppas model[a]

		n					
Kinetic models	Equations	①	②	③	④	⑤	⑥
Korsmeyer–Peppas	(9)	1.4510	1.4950	1.9828	1.2654	2.2737	1.1569

[a] Annotations:①β-CD@5-Fu@ : CCS = 20 : 30; ②β-CD@5-Fu@ : CCS = 15 : 35; ③β-CD@5-Fu@ : CCS = 10 : 40; ④5-Fu@ : CCS = 20 : 30; ⑤5-Fu@ : CCS = 15 : 35; ⑥5-Fu@ : CCS = 10 : 40.

results indicate that throughout the SGF phase, the hydrogel beads maintained their intact morphology and clear granular structure, demonstrating excellent stability in the acidic gastric environment. Upon transfer to the SIF phase, the hydrogel beads retained structural integrity during the first 2 hours. Subsequently, the beads gradually became transparent, and within 2–12 h, the spherical structure disintegrated into gel fragments, at which point the release mechanism was dominated by matrix erosion, followed by the slow release of the drug from the inclusion complex (Fig. 5(f)). This staged degradation profile suggests that the hydrogel beads possess the ability to achieve controlled drug release in the intestinal environment, thereby providing strong support for effective intestinal-targeted drug delivery.

Fig. 5(c and d) present a comparative analysis of the mass loss behavior between hydrogel beads incorporating the β-cyclodextrin@5-fluorouracil complex and those containing free 5-Fu under simulated digestive conditions. Experimental results demonstrate that the β-CD@5-Fu complex system exhibited a mass loss of less than 20% during the simulated gastric fluid phase (0–2 hours). Upon transition to the simulated intestinal fluid phase (2–4 hours), the mass loss progressively increased to a range of 40–60%, reflecting a sustained and controlled release profile.

In contrast, the free 5-Fu system demonstrated substantial mass loss (approximately 30%) in the gastric fluid environment at a drug-to-wall material ratio of 20 : 30, although other ratios maintained mass loss within 20%. However, upon entering the intestinal fluid phase, all formulations rapidly approached near 60% mass loss, displaying steep release kinetics. These observations reveal two key insights: (1) increasing the proportion of wall materials can significantly enhance the hydrogel's barrier properties against digestive fluid erosion; (2) the incorporation of β-cyclodextrin, through its molecular encapsulation mechanism, not only improves the system's resistance to both gastric and intestinal fluids but also achieves controlled release by modulating the drug diffusion pathway. This controlled release behavior is primarily attributed to the confinement of 5-Fu within β-CD's hydrophobic cavity and the associated dissociation kinetics of the inclusion complex.

Fig. 5(b) illustrates the cumulative release rate (CFR%) of β-CD@5-Fu complexes with different wall material ratios at various time intervals. The following key observations can be derived from the data: (1) all formulations demonstrated a gradual increase in release rate during the initial 4 hours period, indicative of controlled and sustained 5-Fu release from the complexes; (2) notably, formulations containing β-CD (β-CD@5-Fu) consistently exhibited lower release rates across all time points compared to those lacking β-CD (free 5-Fu), indicating that β-CD incorporation significantly modulated the release dynamics of 5-Fu. This controlled release mechanism is particularly advantageous in cancer therapy, where precise regulation of drug dosage is essential to minimize cytotoxic effects.[42] Consequently, the introduction of β-CD effectively reduced the release rate of 5-Fu, providing valuable insights for the optimization of drug delivery systems.

Table 3 provides a comprehensive comparison of the developed β-CD@5-Fu/CMCS/CMCNa/SA hydrogel bead system with other reported colon-targeted 5-Fu delivery systems, focusing on encapsulation efficiency, *in vitro* release behavior, and underlying release mechanisms. As summarized in the table, most existing 5-Fu-loaded hydrogel systems—such as P(NVCL-*co*-VIm)/PVP hydrogel, azo hydrogel, pectin-based PPAD hydrogel networks, and 5-FU@β-CD/Alg/CEM formulations—exhibit either relatively high gastric release rates (ranging from 22.79–25%) or excessive colonic/intestinal release rates (up to 100%). These characteristics may lead to premature drug leakage in the upper gastrointestinal tract and insufficient local drug concentrations in the colon. In contrast, the hydrogel beads developed in this work achieve an outstanding encapsulation efficiency of 81.23%, coupled with extremely low release rates of less than 4% in both simulated gastric fluid (pH 1.2) and colonic/intestinal fluid environments (Fig. S3). This superior performance is attributed to the system's unique two-stage

Table 3 Comparison of our system with reported colon-targeted 5-Fu delivery systems

Carrier matrix	Drug	Encapsulation efficiency	Gastric release rate (pH 1.2)	Colonic/Intestinal release rate	Release mechanism	Reference
P(NVCL-*co*-VIm)/PVP hydrogel	5-Fu	80%		~96%	pH-sensitive	39
Azo hydrogel	5-Fu		22.79%	100.00%	pH-responsive + enzyme-responsive	40
Pectin/poly(acrylamide-*co*-(2-dimethylamino)ethyl methacrylate) (PPAD) hydrogel networks	5-Fu	74.3% ± 1.83%		75%	pH-responsive	41
5-FU@β-CD/Alg/CEM	5-Fu		25%	85%	pH-responsive	24
β-CD@5-Fu/CMCS/CMCNa/SA	5-Fu	81.23%	<4%	<4%	Two-stage: pH-responsive hydrogel disintegration + host–guest inclusion complex dissociation	This work

release mechanism: the pH-responsive disintegration of the hydrogel matrix, combined with the dissociation of the host–guest inclusion complex between β-CD and 5-Fu. This dual mechanism effectively prevents premature drug release in the stomach and enables precise, controlled release in the intestinal tract, demonstrating significant advantages over conventional colon-targeted delivery systems that rely on a single release mechanism.

It should be noted that this study has certain limitations. First, although our system exhibits good release stability in simulated gastrointestinal fluids, systematic long-term stability studies (*e.g.*, accelerated testing or long-term storage stability evaluation) have not yet been conducted due to limitations in sample quantity and research timeline. Second, mucoadhesion was not a primary design mechanism of our system; therefore, related *in vitro* or *in vivo* mucoadhesion tests were not performed. Nevertheless, we fully recognize that for colon-targeted delivery systems, mucoadhesive properties may further enhance local retention time and absorption efficiency at the colonic site. Therefore, in future studies, we will systematically carry out the following work: (1) systematically evaluate the long-term stability of the hydrogel beads under different storage conditions (*e.g.*, temperature, humidity, and light exposure); and (2) establish *in vitro* and *in vivo* mucoadhesion evaluation models to explore the colonic mucosal interaction mechanism of our system. These future investigations will provide a more solid experimental basis for the clinical translation of our system.

4 Conclusion

In this study, a 5-fluorouracil-loaded hydrogel beads system based on β-cyclodextrin and polymer composites was successfully developed, followed by systematic evaluation of its physicochemical properties and sustained-release mechanisms. The incorporation of β-CD demonstrated remarkable enhancement in drug loading capacity and encapsulation efficiency. Specifically, the β-CD@5-Fu complex exhibited an encapsulation efficiency of 38.32% and a drug loading capacity of 29.82%. Through rigorous optimization of processing parameters, when the mass ratio of drug complex to wall materials (CMCS/CMCNa/SA) was adjusted to 15 : 35, the resultant hydrogel beads achieved optimal performance, with encapsulation efficiency significantly improved to 81.23%. Drug release kinetics analysis revealed excellent correlation coefficients (R^2 > 0.9) across various models including zero-order, first-order, and Higuchi kinetics, confirming the sustained-release capability of β-CD within a controlled range. This unique characteristic ensures maintenance of stable drug concentration and effectively prevents initial burst release phenomenon. The developed formulation has the potential for application in the local treatment of colorectal cancer.

Author contributions

Conceptualization, Y. W., P. X. and J. L.; methodology, Y. W. and P. X.; validation, Y. W., P. X. and J. L.; formal analysis, Y. W., P. X. and H. L.; investigation, Y. W., P. X. and Q. L.; resources, J. C., Z. L. and Y. L.; data curation, Y. W., P. X. and J. L.; writing – original draft preparation, Y. W. and W. L.; writing – review & editing, J. C. and Y. L.; supervision, J. C., Z. L. and Y. L.; project administration, Y. L.; funding acquisition, Y. L. All authors have read and agreed to the published version of the manuscript.

Conflicts of interest

The authors declare no competing interests.

Data availability

The authors declare that they have no known competing financial interests or personal relationships that could have appeared to influence the work reported in this paper.

Supplementary information (SI) is available. See DOI: https://doi.org/10.1039/d6ra00194g.

Acknowledgements

This work was sponsored by Fuzhou Marine Research Institute 'Unveiling the List and Entrusting the Best Candidate' Project (2024F12), Fujian Provincial Natural Science Foundation (2025J08275), Fujian provincial health technology project (2023CXA008), Natural Science Foundation of Fujian Province of China (2024J011000), Fujian Provincial Science and Technology Department Health Joint Climbing Program

(2024Y9003), Guiding Project of Fujian Provincial Department of Science and Technology (No. 2020Y0019), Fujian Provincial Science and Technology Department Spark project (2022S0012), Fushimei Agricultural and rural maker space (Minke xing [2019] No. 2), Program for Innovative Research Team in Science and Technology in Fujian Province University, Fuzhou characteristic herbal resources sustainable development industry technology innovation center, 2024 National Student Innovation and Entrepreneurship Training Programme Project Funding(202410394017), Fujian Normal University "Innovation and Entrepreneurship Training Program for College Students" Innovation Training Category (S202510394017).

References

1 F. A. Khan, R. Albalawi and F. H. Pottoo, *Med. Res. Rev.*, 2021, **42**, 227–258.
2 Z. Bugra, A. Mohammad and A. D. Lisa, *J. Clin. Oncol.*, 2025, **43**, 300.
3 F. Qian, H. Xiaoying, F. Limei, D. Yufei, L. Xiaoxuan, Z. Hongyun, W. Haiping, F. Zhengqi, S. Binlian, S. Xiji, D. Hongzhi and L. Yuchen, *Pharmacol. Res.*, 2025, **213**, 1–15.
4 A. Azevedo, M. P. Coelho, J. O. Pinho, P. I. P. Soares, C. P. Reis, J. P. Borges and M. M. Gaspar, *Life Sci.*, 2024, **344**, 122558.
5 W. Chen, K. Shi, J. Liu, P. Yang, R. Han, M. Pan, L. Yuan, C. Fang, Y. Yu and Z. Qian, *Bioact. Mater.*, 2022, **23**, 1–15.
6 X. Deng, Z. Yang, K. W. Chan, N. Ismail and M. Z. Abu Bakar, *Antioxidants*, 2024, **13**, 1030.
7 P. Sara, F. Amin, P. Mehrab and A. Majid, *Results Chem.*, 2024, **12**, 1–17.
8 S. Jie, W. Youqian, N. Yuhua, H. Baoli and W. Haodi, *Int. J. Biol. Macromol.*, 2024, **280**, 1–11.
9 F. Wang, Y. Song, J. Huang, B. Wu, Y. Wang, Y. Pang, W. Zhang, Z. Zhu, F. Ma, X. Wang and X. Zhang, *Macromol. Biosci.*, 2021, **21**, 1–10.
10 Z. Han, P. Wang, G. Mao, T. Yin, D. Zhong, B. Yiming, X. Hu, Z. Jia, G. Nian, S. Qu and W. Yang, *ACS Appl. Mater. Interfaces*, 2020, **12**, 12010–12017.
11 Z. Jianxi, T. Junjie, S. Si, H. Jiaxin, L. Wenhao, L. Yuanzhao, Z. Xinxin, P. Jie and W. Chunhua, *Food Hydrocolloids*, 2025, **163**, 1–10.
12 L. Xinxin, L. Longhai, H. Fang, M. Yanmei, C. Yajuan, W. Jianqiang, W. Shuang, L. Yangchao, L. Jianghua and L. Ying, *Food Chem.*, 2024, **470**, 1–10.
13 C. Yue and G. Zhang, *J. Environ. Chem. Eng.*, 2022, **10**, 1–9.
14 H. Jing, X. Huang, X. Du, L. Mo, C. Ma and H. Wang, *Carbohydr. Polym.*, 2021, **278**, 1–10.
15 Y. Sheng, J. Gao, Z.-Z. Yin, J. Kang and Y. Kong, *Carbohydr. Polym.*, 2021, **269**, 1–8.
16 L. Fan, Y. Du, B. Zhang, J. Yang, J. Zhou and J. F. Kennedy, *Carbohydr. Polym.*, 2006, **65**, 447–452.
17 L. Wu, Y. Hu, P. Tang, H. Wang and Y. Bin, *Compos. Commun.*, 2021, **24**, 1–6.
18 G. Jun, W. Rongzhi, L. Zhengyin, Z. Zherui, K. Yong and Z. Min, *ACS Appl. Nano Mater.*, 2025, **8**, 3688–3696.
19 F. Niu, D. Hu, F. Gu, Y. Du, B. Zhang, S. Ma and W. Pan, *Carbohydr. Polym.*, 2021, **271**, 1–8.
20 R. Zhao, B. Tang, Z. Xu and G. Fang, *Coord. Chem. Rev.*, 2025, **534**, 216581.
21 S. Payamifar, A. Foroozandeh, M. Pourmadadi and M. Abdouss, *Results Chem.*, 2024, **12**, 101878.
22 M. R. Abukhadra, A. T. Okasha, S. I. Al Othman, H. E. Alfassam, N. A. Alenazi, A. A. AlHammadi and A. A. Allam, *ACS Omega*, 2023, **8**, 30247–30261.
23 Y. Fan, D. Shen, Y. Yan, X. Hu, Y. Guo, Y. Zhong, Z. Li and L. Xie, *J. Polym. Environ.*, 2022, **30**, 4863–4876.
24 M. Anoosh, S. A. Ghumman, H. Hameed, S. Noureen, R. Kausar, A. Irfan, M. A. A. Alrobesh, M. Arshad, P. A. Shah, M. Rana and Y. A. Bin Jardan, *RSC Adv.*, 2026, **16**, 642–656.
25 H. Ghasemizadeh, M. Pourmadadi, F. Yazdian, H. Rashedi, M. Navaei-Nigjeh, A. Rahdar and A. M. Díez-Pascual, *Int. J. Biol. Macromol.*, 2023, **232**, 1–12.
26 W. Bai, M. Li, J. Li, W. Cai, Y. Kong and H. Chen, *Mol. Pharm.*, 2026, **23**, 1758–1769.
27 D. L. Melnikova, Z. F. Badrieva, M. A. Kostin, C. Maller, M. Stas, A. Buczek, M. A. Broda, T. Kupka, A.-M. Kelterer, P. M. Tolstoy and V. D. Skirda, *Molecules*, 2020, **25**, 1–18.
28 B. Zhang, C. Hu, M. Wang, H. Wei, S. Li, H. Yu, Y. Wu, G. Wang, T. Guo and H. Chen, *J. Colloid Interface Sci.*, 2024, **678**, 827–841.
29 N. Poursharifi, D. Semnani, P. Soltani and S. Amanpour, *Polym. Degrad. Stab.*, 2020, **179**, 1–10.
30 A. Abou-Okeil, M. Rehan, S. M. El-Sawy, M. K. El-bisi, O. A. Ahmed-Farid and F. A. Abdel-Mohdy, *Eur. Polym. J.*, 2018, **108**, 304–310.
31 M. Parsaei and K. Akhbari, *Inorg. Chem.*, 2022, **61**, 5912–5925.
32 J. Gao, Y. Sang, X. Han, Y. Zhao, T. Liang and T. Chen, *J. Saudi Chem. Soc.*, 2024, **28**, 1–10.
33 H. M. El-Zeiny, M. R. Abukhadra, O. M. Sayed, A. H. M. Osman and S. A. Ahmed, *Colloids Surf., A*, 2020, **586**, 1–11.
34 L. Zhang, J. Zhou and L. Zhang, *Carbohydr. Polym.*, 2013, **94**, 386–393.
35 S. Pereva, V. Nikolova, S. Angelova, T. Spassov and T. Dudev, *Beilstein J. Org. Chem.*, 2019, **15**, 1592–1600.
36 L. X. Song, C. F. Teng, P. Xu, H. M. Wang, Z. Q. Zhang and Q. Q. Liu, *J. Incl. Phenom. Macrocycl. Chem.*, 2008, **60**, 223–233.
37 Z. Ying, W. Yinqi, L. Huize, L. Bin, J. Wendan, W. Sainan, L. Bo and Y. Hansong, *Food Hydrocolloids*, 2025, **164**, 1–9.
38 Z. Yuxin, Y. Guanglong, L. Kaimian, Y. Jianqiu, C. Jian and Z. Jie, *Food Chem.:X*, 2024, **25**, 1–10.
39 A. Güngör, T. Özdemir and R. Genç, *Polym. Bull.*, 2024, **81**, 2091–2109.
40 Z. Ma, R. Ma, X. Wang, J. Gao, Y. Zheng and Z. Sun, *Eur. Polym. J.*, 2019, **118**, 64–70.
41 S. Eswaramma, N. S. Reddy and K. S. V. K. Rao, *Int. J. Biol. Macromol.*, 2017, **103**, 1162–1172.
42 G. Raffaini, S. Elli, M. Catauro and A. D'Angelo, *Int. J. Mol. Sci.*, 2024, **25**, 1–25.